INTERNATIONAL JOURNAL FOR NUMERICAL METHODS IN FLUIDS, VOL. 17, 301–321 (1993)

BENCHMARK SOLUTIONS FOR THE INCOMPRESSIBLE NAVIER–STOKES EQUATIONS IN GENERAL CO-ORDINATES ON STAGGERED GRIDS

C. W. OOSTERLEE, P. WESSELING, A. SEGAL AND E. BRAKKEE

Faculty of Technical Mathematics and Informatics, Delft University, P.O. Box 5031, 2600 GA Delft, The Netherlands

SUMMARY

Benchmark problems are solved with the steady incompressible Navier–Stokes equations discretized with a finite volume method in general curvilinear co-ordinates on a staggered grid. The problems solved are skewed driven cavity problems, recently proposed as non-orthogonal grid benchmark problems. The system of discretized equations is solved efficiently with a non-linear multigrid algorithm, in which a robust line smoother is implemented. Furthermore, another benchmark problem is introduced and solved in which a 90° change in grid line direction occurs.

KEY WORDS Benchmark solution Incompressible Navier–Stokes Staggered grid General co-ordinates Multigrid

1. INTRODUCTION

In recent years several methods have been proposed for the discretization and the solution of the incompressible Navier–Stokes equations in arbitrarily shaped domains with a finite difference or a finite volume method. Most publications adopt a boundary-fitted curvilinear co-ordinate system. The discretization methods which employ curvilinear co-ordinate systems differ in grid arrangement (staggered or non-staggered grids), and in choice of velocity components (Cartesian or so-called grid-oriented velocity unknowns, such as contravariant components). A brief overview of some important groups solving the incompressible Navier–Stokes equations is given here. A distinction is made between groups solving the incompressible Navier–Stokes equations in general co-ordinates on staggered and colocated grids and researchers using a pseudo-compressibility approach. First, investigations on colocated grids with Cartesian velocity components as dependent variables and transformed velocity components as independent variables are enumerated. In Reference 1 this choice is made, where further a comparison is given between the several choices to be made to get accurate discretizations. The pioneering papers of the colocated approach are by Rhie *et al.*[2,3] A lot of research on discretizations for non-staggered grids with Cartesian velocity unknowns is also presented in References 4–6, where the set of benchmark solutions discussed here is proposed for incompressible Navier–Stokes equations in non-orthogonal domains. Other papers based on the colocated approach are References 7 and 8 where results with advanced upwind schemes on colocated grids and fast solution methods are obtained. In Reference 9 non-staggered grids are adopted to investigate the effect of several upwind schemes

0271–2091/93/160301–21$15.50

Received 10 September 1992
Revised 11 February 1993

and turbulence models on the convergence of a multigrid solution technique for the incompressible Navier–Stokes equations. Some commercial codes have adopted colocated grids for solutions of complex flows in arbitarily shaped domains.[10] A second group of researchers adopt pseudo-compressibility methods. With an artificial time-dependent pressure term in the continuity equation the incompressible Navier–Stokes equations can be approached with methods from compressible Navier–Stokes equations. All unknowns are also stored in the centres of grid cells; Cartesian velocity components and pressure are dependent variables. This method is, for example, adopted for discretizations in curvilinear co-ordinates by Kwak *et al.*[11,12] An advanced upwind scheme based on flux difference splitting is incorporated in Reference 12.

Discretizations on staggered grids are also applied on a large scale. Interesting papers have been published by Rosenfeld *et al.*,[13–15] where on a staggered grid contravariant fluxes V^α and pressures are used as primary unknowns. Two- and three-dimensional results with moving grids and multigrid acceleration are described in these papers. In Japan, staggered grids are widely investigated in Reference 16 for two-dimensional and in Reference 17 for three-dimensional problems with dependent variables contravariant fluxes V^α and contravariant vorticities. In Reference 18 contravariant physical components and pressure are used as unknowns. A similar approach using the same unknowns can be found in Reference 19.

Some other papers will be mentioned briefly. An analysis of the treatment of a pressure equation on a curvilinear staggered grid is presented in Reference 20. In Reference 21 the stability problems on staggered grids with Cartesian velocity components are investigated and remedies are given. In Reference 22 the staggered approach is chosen for solving incompressible Navier–Stokes equations in curvilinear co-ordinates, because of the merits in boundary treatment, the compactness of effective mesh spacing, and the insensitivity of solutions with respect to the values of relaxation factors used in the iterative procedure. Approaches different from all others are described in Reference 23, where on a staggered grid covariant velocity components are used to solve the incompressible Navier–Stokes equations, and in Reference 24, where a rectangular co-ordinate system is used with special treatment for the boundaries. In our group progress has been made with the discretization of the steady and unsteady incompressible Navier–Stokes equations in general co-ordinates using a finite volume method on a staggered grid.[25–27] Accurate results were obtained with Dirichlet boundary conditions[28,29] for the steady equations with a multigrid solution method and also for the unsteady equations using (semi-) natural boundary conditions[26] with a pressure correction method and a GMRES solver. The incompressible Navier–Stokes equations were discretized on a staggered grid with contravariant fluxes V^α and pressure as primary unknowns.

Recently, two benchmark problems were proposed in Reference 6 for discretizations on non-orthogonal grids in two dimensions in order to compare different discretization methods. The Navier–Stokes equations were solved on a non-staggered grid with Cartesian velocity unknowns; the discretization is described in Reference 5. The solution method is a SIMPLE-type method.[30,31] Discretization in general co-ordinates on a staggered grid is a far from trivial matter, and may be very inaccurate, unless certain precautions are taken, discussed in References 25 and 26. In order to validate our approach, in the present paper the benchmark problems of Reference 6 are solved with our steady variant. A steady-state multigrid solution method is used in which velocity and pressure are solved in a coupled technique by means of the Symmetric Coupled Alternating Lines (SCAL) smoothing method.[32] Furthermore, a third benchmark problem is introduced and solved. In this problem a 90° change in grid line direction occurs, a situation which is difficult to handle with Cartesian velocity components as unknowns, and brings out the advantage of the co-ordinate-invariant approach of References 25 and 26 and the present paper.

2. THE INCOMPRESSIBLE NAVIER–STOKES EQUATIONS IN GENERAL CO-ORDINATES

The fundamentals of tensor analysis, especially in relation to continuum mechanics, are presented in textbooks such as Aris[33] and Sokolnikoff.[34] The discretization is described in more detail in References 26, 29 and 35.

In general co-ordinates the steady incompressible Navier–Stokes equations are given by

$$U^{\alpha}_{,\alpha}=0, \tag{1}$$

$$T^{\alpha\beta}_{,\beta}\equiv(\rho U^{\alpha}U^{\beta})_{,\beta}+(g^{\alpha\beta}p)_{,\beta}-\tau^{\alpha\beta}_{,\beta}=\rho F^{\alpha}, \tag{2}$$

where $\tau^{\alpha\beta}$ represents the deviatoric stress tensor given by

$$\tau^{\alpha\beta}=\mu(g^{\alpha\gamma}U^{\beta}_{,\gamma}+g^{\gamma\beta}U^{\alpha}_{,\gamma}). \tag{3}$$

Here U^{α} are contravariant velocity components, ρ is density, p is pressure and μ is the viscosity coefficient. Unknowns $V^{\alpha}=\sqrt{g}\,U^{\alpha}$ are used as primary unknowns together with the pressure. The arbitrarily shaped flow domain Ω is mapped onto a rectangular block G, resulting in boundary-fitted co-ordinates. The co-ordinate transformation is given by $\mathbf{x}=\mathbf{x}(\boldsymbol{\xi})$, with $\mathbf{x}$ Cartesian co-ordinates and $\boldsymbol{\xi}$ boundary conforming curvilinear co-ordinates. The covariant derivative formula used for the continuity equation is

$$U^{\alpha}_{,\alpha}=\frac{1}{\sqrt{g}}\frac{\partial\sqrt{g}\,U^{\alpha}}{\partial\xi^{\alpha}}. \tag{4}$$

Terms in the momentum equations of the type $T^{\alpha\beta}_{,\beta}$ are given by

$$T^{\alpha\beta}_{,\beta}=\frac{1}{\sqrt{g}}\frac{\partial\sqrt{g}\,T^{\alpha\beta}}{\partial\xi^{\beta}}+\begin{Bmatrix}\alpha\\ \gamma\beta\end{Bmatrix}T^{\gamma\beta}, \tag{5}$$

where $\{^{\alpha}_{\gamma\beta}\}$ represents the Christoffel symbol of the second kind.

The equations are discretized with a finite volume method on a uniform staggered grid in G. We introduce local cell co-ordinates given by Figure 1, which shows part of the computational grid in the ξ-plane. Taking a cell with centre at V^1-point (1, 0) as an example, finite volume discretization gives, using (5)

$$\int_{\Omega}T^{1\beta}_{,\beta}\,\mathrm{d}\Omega=\int_{\Omega}\frac{\partial\sqrt{g}\,T^{1\beta}}{\partial\xi^{\beta}}\,\mathrm{d}\xi^{1}\,\mathrm{d}\xi^{2}+\int_{\Omega}\begin{Bmatrix}1\\ \gamma\beta\end{Bmatrix}T^{\gamma\beta}\sqrt{g}\,\mathrm{d}\xi^{1}\,\mathrm{d}\xi^{2}$$

$$\cong(\sqrt{g}\,T^{11})\Big|^{2;0}_{0;0}\delta\xi^{2}+(\sqrt{g}\,T^{12})\Big|^{1;1}_{1;-1}\delta\xi^{1}+\left(\sqrt{g}\begin{Bmatrix}1\\ \gamma\beta\end{Bmatrix}T^{\gamma\beta}\Big|_{1,0}\right)\delta\xi^{1}\delta\xi^{2}. \tag{6}$$

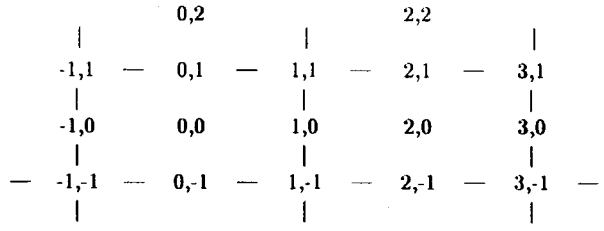

Figure 1. Local cell co-ordinates

The second component of (2) is similarly approximated with a cell centred at a V^2-point. With $T^{\alpha\beta}_{,\beta}$ from (2) this is the discretization used for the momentum equations. It is found that the variable $V^\alpha = \sqrt{g}U^\alpha$ appears naturally in many places in (6). The convection tensor is linearized using a Picard iteration

$$(\rho U^\alpha U^\beta)_{,\beta} \simeq (\rho U^{\alpha(n+1)} U^{\beta(n)})_{,\beta}, \tag{7}$$

where the superscript n is an iteration index.

The convection term is discretized with the so-called hybrid discretization scheme.[30,31] Depending on the mesh Reynolds number $Re^{(i,j)}$ (i.e. the ratio between the absolute magnitudes of the flux part of the convection term and the viscous term in point (i,j)), the flux part of the convection term is discretized with a central difference scheme (when $Re^{(i,j)} < 1$) or with a first-order upwind scheme (when $Re^{(i,j)} > 1$). There is a smooth switch between the two schemes using a smooth switching function $\omega(Re^{(i,j)})$.

The total number of variables linked together in a momentum equation is 19. The discretized equations are solved with the standard non-linear multigrid method.[36,37] Details are presented in References 38 and 29. Here the smoothing method called SCAL[32,35] is described briefly.

All velocity components and pressures in a line of cells are updated simultaneously. This is a line-by-line version of the cell-by-cell smoother SCGS introduced in Reference 39, a so-called coupled smoothing method, because different unknowns (velocity components and pressure) are solved simultaneously. SCGS is used as smoothing method for discretizations in curvilinear co-ordinates in References 40 and 29. The smoother SCAL is much more robust than SCGS. Many problems in arbitrary domains, where cells with large aspect ratio occur have been solved successfully.[35]

For each line a banded system is solved and intermediate values (V^{1*}, V^{2*}, p^*) are obtained. With underrelaxation the new values ($V^{1(n+1)}$, $V^{2(n+1)}$, $p^{(n+1)}$) are found. After an update of unknowns along horizontal lines, unknowns are updated again using vertical lines. SCAL is a zebra-type smoother: first all odd (white) lines are visited, then all even (black) lines are visited. With special ordering strategies acceleration can be obtained on vector computers.

3. BENCHMARK SOLUTIONS

In Reference 6 two benchmark problems are defined for discretizations on non-orthogonal grids. The flow problems are skewed-driven cavity problems. The domain, depicted in Figure 2, is a parallelogram with boundary length $L = 1$. Angle β is 45° for case 1, and 30° for case 2, so that highly non-orthogonal cells occur in the x-image of the grid. The top wall is moving with Cartesian velocity components $u^1 = 1$, $u^2 = 0$. On all other boundaries $\mathbf{u} = 0$ is prescribed. The flow problems are calculated for Reynolds numbers (Re) 100 and 1000. The discretization is investig-

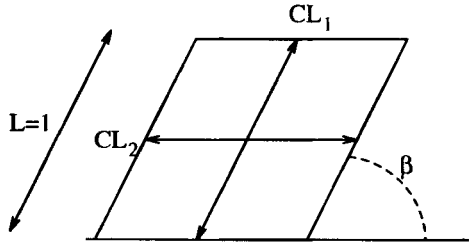

Figure 2. Domain for the skewed-driven cavity problem

ated on four grids, consisting of 32×32, 64×64, 128×128 and 256×256 cells, respectively. The streamline patterns obtained agree closely with those in Reference 6. They are presented in Figure 3 for $\beta = 45°$, in Figure 4 for $\beta = 30°$. The prescribed streamline values in these figures are identical to those in Reference 6. The maximum and minimum values of the stream function Ψ_{max} and Ψ_{min} are determined for all grids together with their co-ordinates (x^1_{min}, x^2_{min}) and (x^1_{max}, x^2_{max}) and an error measure ε, defined as in Reference 6:

$$\varepsilon = \left| \frac{\Psi_{256} - \Psi_{128}}{\Psi_{256}} \right| \cdot 100. \tag{8}$$

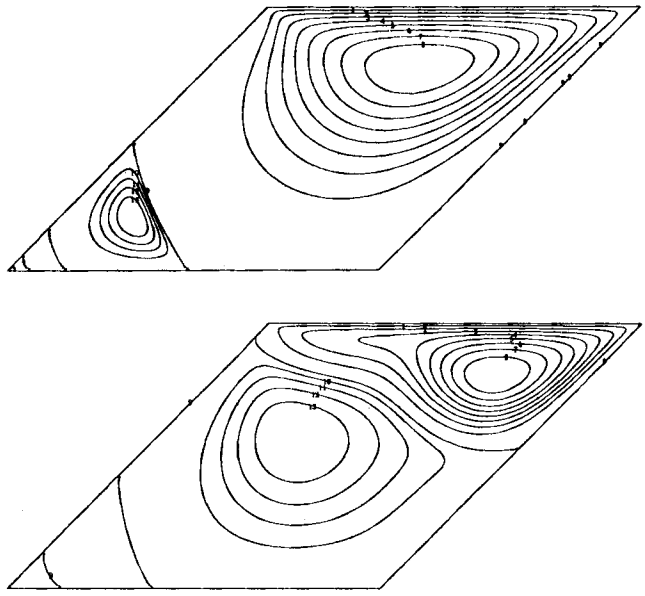

Figure 3. Streamlines for $Re = 100$ and $Re = 1000$ for testcase 1

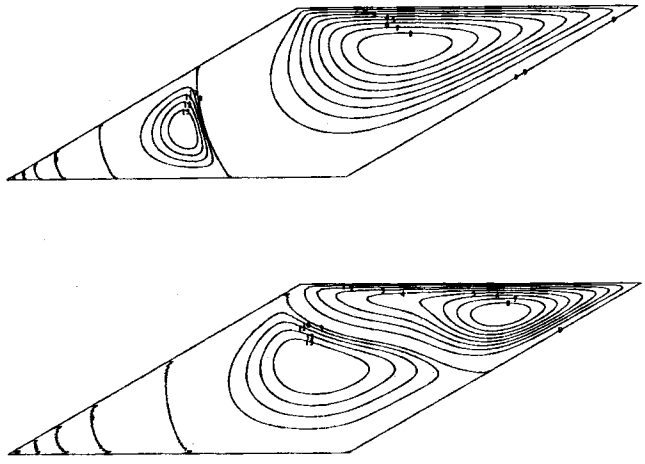

Figure 4. Streamlines for $Re = 100$ and $Re = 1000$ for testcase 2

Table I. Minimum and maximum stream function values in vortex centres and their position for all grids and for both Reynolds numbers, skewed cavity, $\beta = 45°$

$\beta = 45°$	$Re = 100$		$Re = 1000$	
	Min	Max	Min	Max
32×32				
Ψ	$-7{\cdot}0260 \times 10^{-2}$	$5{\cdot}6150 \times 10^{-5}$	$-4{\cdot}6914 \times 10^{-2}$	$7{\cdot}3515 \times 10^{-3}$
x	1·1149	0·3422	1·2933	0·7415
y	0·5524	0·1547	0·5745	0·3978
64×64				
Ψ	$-7{\cdot}0266 \times 10^{-2}$	$4{\cdot}1058 \times 10^{-5}$	$-5{\cdot}1778 \times 10^{-2}$	$8{\cdot}6275 \times 10^{-3}$
x	1·1039	0·3468	1·3089	0·7682
y	0·5414	0·1436	0·5745	0·4088
128×128				
Ψ	$-7{\cdot}0253 \times 10^{-2}$	$3{\cdot}7725 \times 10^{-5}$	$-5{\cdot}3456 \times 10^{-2}$	$1{\cdot}0024 \times 10^{-2}$
x	1·1094	0·3401	1·3089	0·7783
y	0·5496	0·1436	0·5745	0·4033
256×256				
Ψ	$-7{\cdot}0238 \times 10^{-2}$	$3{\cdot}6932 \times 10^{-5}$	$-5{\cdot}3523 \times 10^{-2}$	$1{\cdot}0039 \times 10^{-2}$
x	1·1100	0·3390	1·3128	0·7775
y	0·5469	0·1409	0·5745	0·4005
ε	0·0214	2·1472	0·1252	0·1494

Table II. Minimum and maximum stream function values in vortex centres and their position for all grids and for both Reynolds numbers, skewed cavity, $\beta = 30°$

$\beta = 30°$	$Re = 100$		$Re = 1000$	
	Min	Max	Min	Max
32×32				
Ψ	$-5{\cdot}3045 \times 10^{-2}$	$1{\cdot}5597 \times 10^{-4}$	$-3{\cdot}7309 \times 10^{-2}$	$4{\cdot}2221 \times 10^{-3}$
x	1·1808	0·5519	1·4537	0·8976
y	0·3750	0·1563	0·4063	0·2656
64×64				
Ψ	$-5{\cdot}3126 \times 10^{-2}$	$7{\cdot}4524 \times 10^{-5}$	$-3{\cdot}8833 \times 10^{-2}$	$4{\cdot}4938 \times 10^{-3}$
x	1·1651	0·3750	1·4537	0·8997
y	0·5384	0·1484	0·4063	0·2578
128×128				
Ψ	$-5{\cdot}3152 \times 10^{-2}$	$5{\cdot}9527 \times 10^{-5}$	$-3{\cdot}8698 \times 10^{-2}$	$4{\cdot}2446 \times 10^{-3}$
x	1·1719	0·5316	1·4526	0·8997
y	0·3789	0·1445	0·4102	0·2578
256×256				
Ψ	$-5{\cdot}3149 \times 10^{-2}$	$5{\cdot}6228 \times 10^{-5}$	$-3{\cdot}8600 \times 10^{-2}$	$4{\cdot}1657 \times 10^{-3}$
x	1·1680	0·5291	1·4565	0·9036
y	0·3789	0·1426	0·4102	0·2559
ε	0·0060	5·8672	0·2539	1·8940

These values are presented in Table I for $\beta = 45°$ and in Table II for $\beta = 30°$. Results agree well with Reference 6. The local error is less than 0·03 per cent of the maximum of the absolute values of Ψ over the domain for $\beta = 45°$ and less than 0·1 per cent for $\beta = 30°$. For $Re = 100$ the results on all grids are accurate. The values for the 128×128- and the 256×256-grid do not differ much for $Re = 1000$. This indicates that the exact solution is closely approximated on these grids. This is also true for velocity profiles along the centrelines CL_1 and CL_2 (Figure 2). Figure 5(a) shows the Cartesian velocity component u^1 along line CL_1 for $Re = 100$, $\beta = 45°$; Figure 5(b) gives u^2 along CL_2. Figure 6(a) shows u^1 along line CL_1 for $Re = 1000$, $\beta = 45°$; Figure 6(b) presents u^2 along CL_2. Figure 7(a) shows u^1 along line CL_1 for $Re = 1000$, $\beta = 30°$; Figure 7(b) presents u^2 along CL_2. For $Re = 100$ all curves are identical; therefore, the velocity profiles for testcase 2 are not shown. This indicates that we have an accurate solver; for a small number of unknowns accurate results are obtained for low Reynolds numbers.

Again for $Re = 1000$ the finest two grids show identical results. On the other grids the effect of the upwind part of the hybrid difference scheme can be observed; differences can be seen mainly in the high-velocity regions. Due to these satisfactory results the discretization is called accurate; similar results were found when other benchmark problems in rectangular domains[41,42] were solved.

Next, the results for the multigrid solution method are presented for these testcases. Average reduction factors μ_{nit} are calculated, defined as

$$\mu_{\text{nit}} = \left(\frac{\| \text{res}_{\text{nit}} \|}{\| \text{res}_1 \|} \right)^{(1/\text{nit}-1)}, \tag{9}$$

with $\| \cdot \|$ the Euclidean norm, and res_n the residual after n iterations. We also give

$$\nu_n \equiv \left\| \frac{\text{res}_n}{\text{res}_{n-2}} \right\|^{1/2} \quad \text{for } n = \text{nit}. \tag{10}$$

In many cases ν_n is found to be approximately constant for n close to nit, in which case we have found the asymptotic convergence factor $\mu_\infty \cong \nu_{\text{nit}}$. The number of MG iterations that were performed depended on the reduction factor μ_{nit}, as follows:

$$\begin{aligned} 0{\cdot}15 < \mu_{\text{nit}} \leq 0{\cdot}3, \quad & \text{nit} \leq 20 \\ \mu_{\text{nit}} > 0{\cdot}3, \quad & \text{nit} \geq 25, \end{aligned} \tag{11}$$

The multigrid cycle used is the F-cycle, because it showed reduction factors comparable to the W-cycle, while it is much cheaper than the W-cycle. The even cheaper V-cycle sometimes showed bad reduction factors for $Re = 1000$ on very fine grids. The number of pre-smoothing iterations and the number of post-smoothing iterations is 1. The coarsest grid always is the 2×2 grid, where 10 smoothing iterations are performed. The number of multigrid levels differed for the different grids from 5 to 8. Table III presents μ_{nit} and ν_{nit} for testcases 1 and 2. The CPU times for one F-cycle on a Convex 3820 computer are presented in Table IV. No parallelization statements or special ordering strategies for vectorization purposes are implemented in the code.

We introduce another benchmark problem, because the grids of testcases 1 and 2 mainly test the effect of non-orthogonality of co-ordinates. In order to also include the effect of curvature of co-ordinate lines (such testcases are also presented in Reference 6, but only for buoyancy driven flows), we propose the problem of flow in an L-shaped-driven cavity. This test problem is not only interesting for testing discretizations, but also for domain decomposition techniques, as used in Reference 43. The domain is depicted in Figure 8. It can be seen in Figure 8 that boundaries

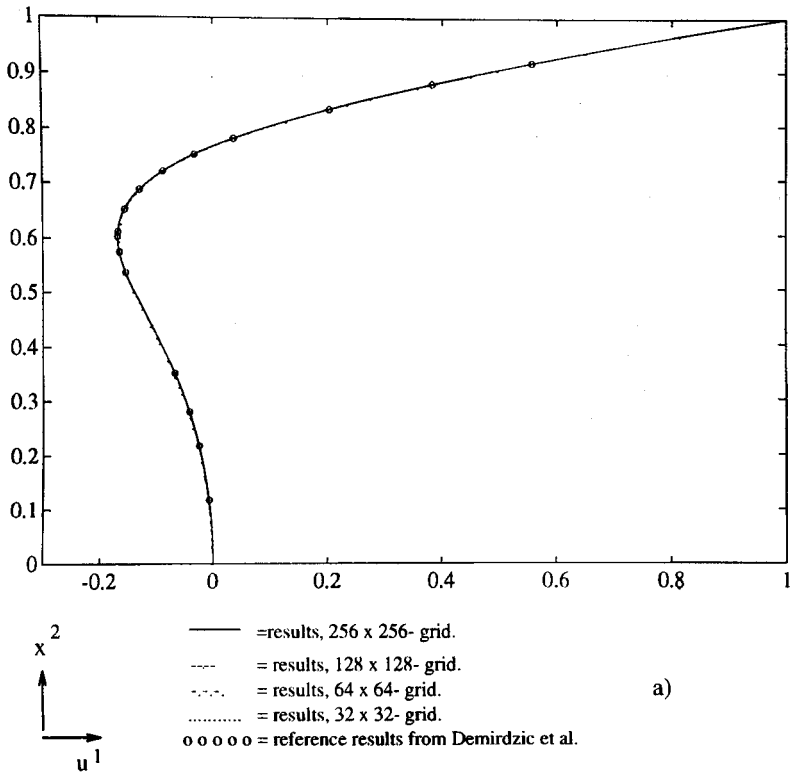

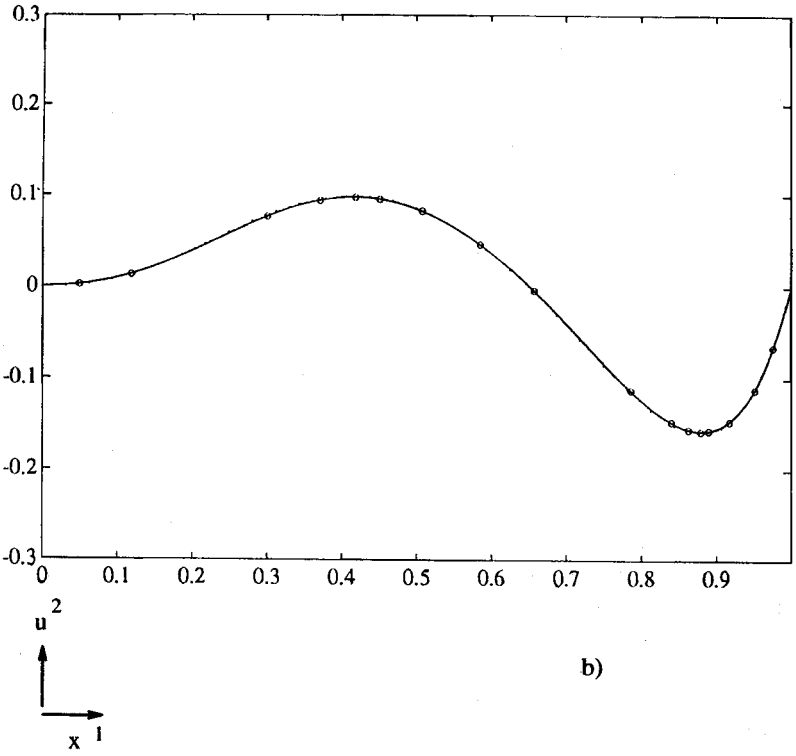

Figure 5. Velocity profiles for $\beta = 45°$: $Re = 100$: (a) u^1 along CL_1; (b) u^2 along CL_2

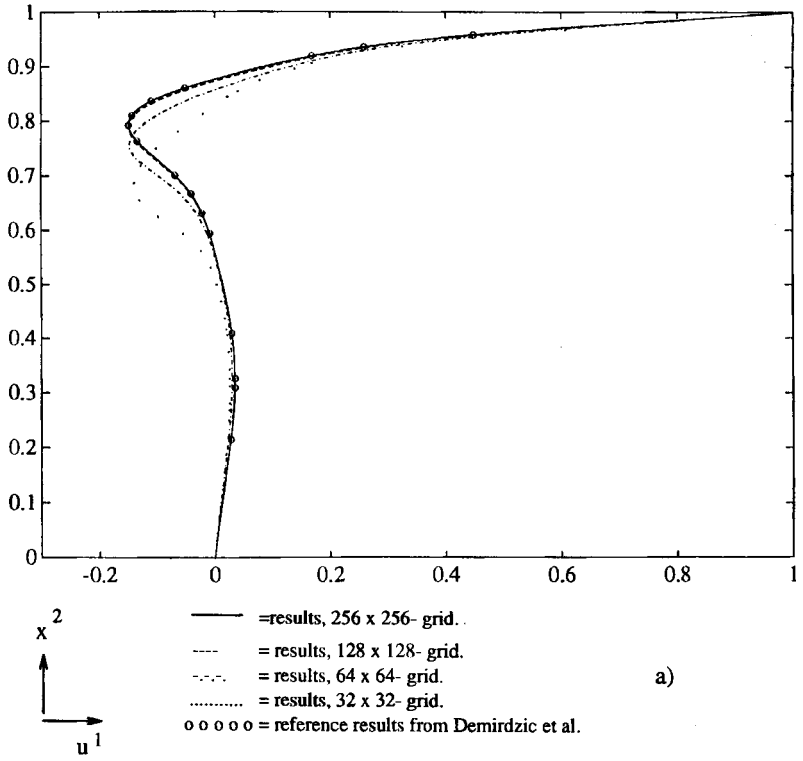

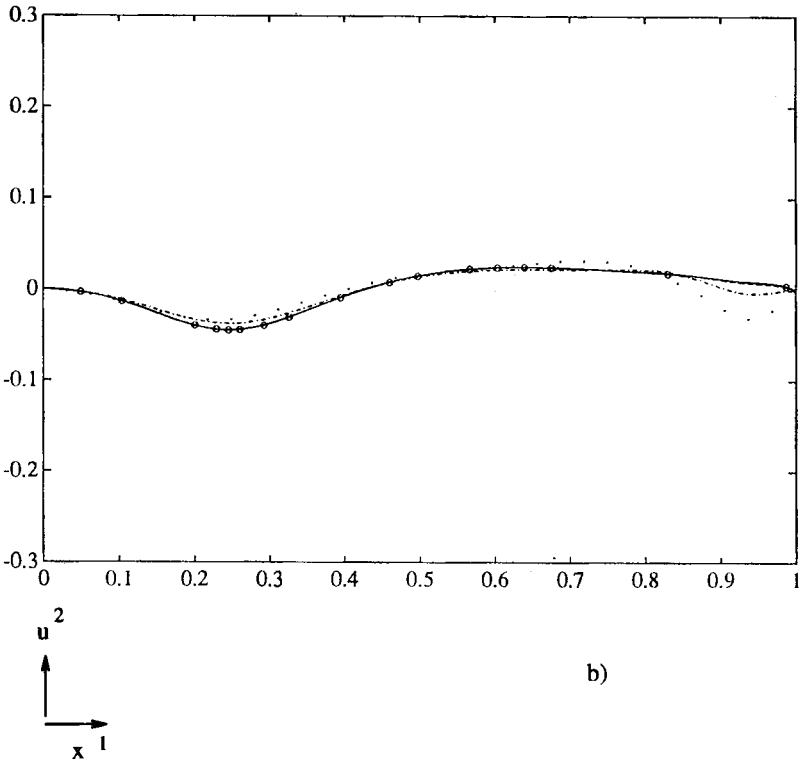

Figure 6. Velocity profiles for $\beta = 45°$: $Re = 1000$; (a) u^1 along CL_1; (b) u^2 along CL_2

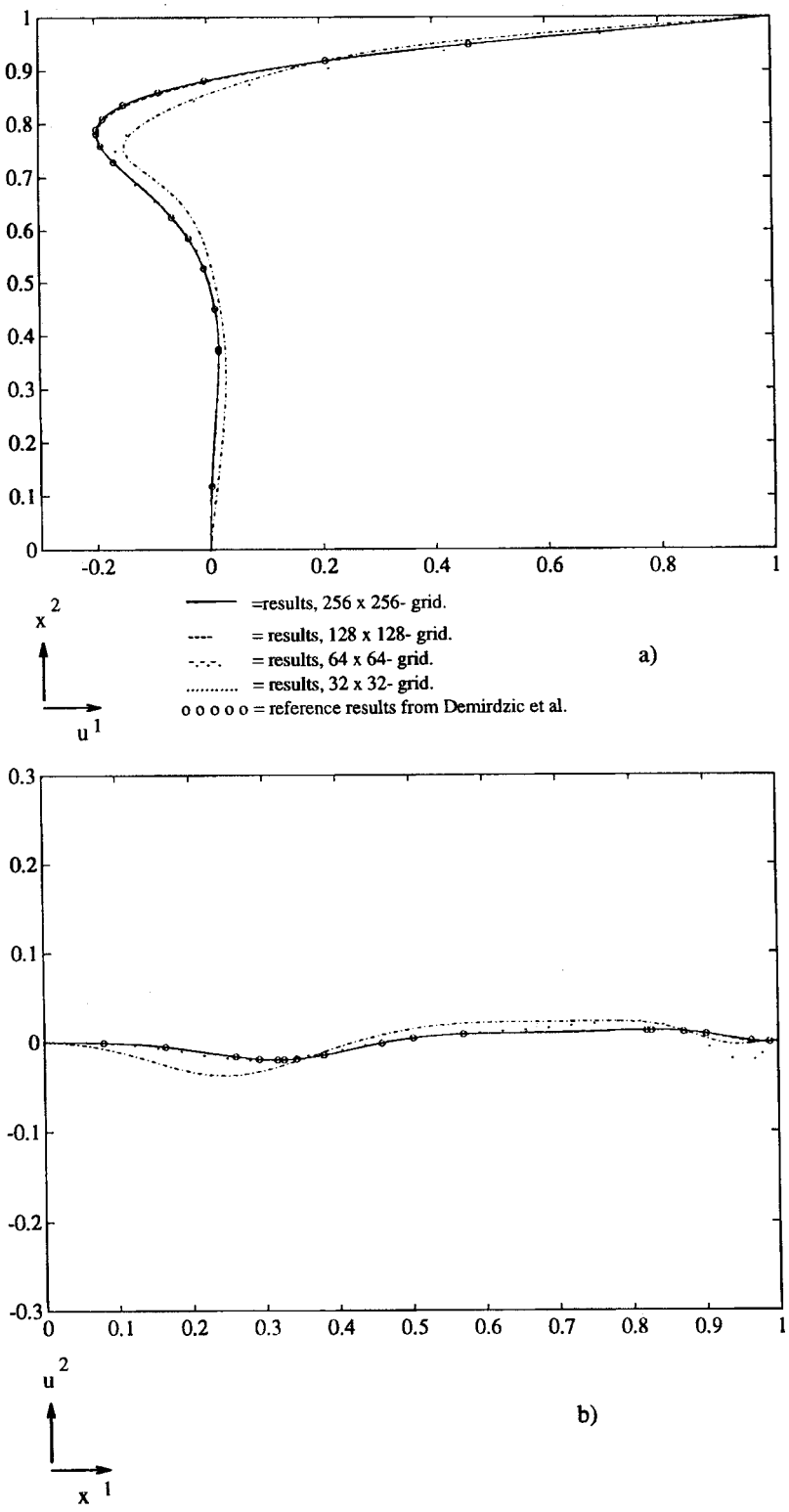

Figure 7. Velocity profiles for $\beta = 30°$: $Re = 1000$: (a) u^1 along CL_1; (b) u^2 along CL_2

Table III. Average and asymptotic reduction factors for skewed-driven cavity problems

Angle	$\beta=45°$				$\beta=30°$			
Reynolds number	100		1000		100		1000	
	μ_{nit}	ν_{nit}	μ_{nit}	ν_{nit}	μ_{nit}	ν_{nit}	μ_{nit}	ν_{nit}
32×32 grid	0·191	0·221	0·617	0·695	0·304	0·373	0·629	0·674
64×64 grid	0·184	0·248	0·712	0·718	0·336	0·412	0·533	0·589
128×128 grid	0·198	0·253	0·718	0·791	0·345	0·428	0·530	0·607
256×256 grid	0·194	0·250	0·604	0·719	0·352	0·431	0·445	0·555

Table IV. CPU times for an F-cycle on a Convex 3820

Grid	32×32	64×64	128×128	256×256	512×512
CPU times	1·34 s	4·67 s	17·4 s	75·2 s	350·0 s

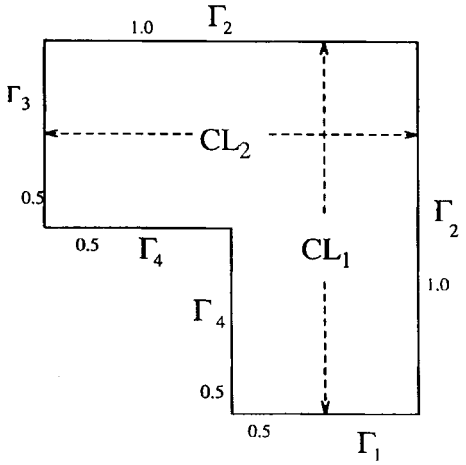

Figure 8. The domain for an L-shaped cavity problem

Γ_2 and Γ_4 consist of two parts. On the upper part of Γ_2 $u^1=1$, $u^2=0$ is prescribed, on all other boundary parts we have $\mathbf{u}=0$. The Reynolds numbers investigated are again 100 and 1000. If the grid is non-smooth, like the one shown in Figure 9, our discretization is not accurate for high Reynolds numbers ($Re=1000$). Figure 10 shows for this grid streamlines for $Re=100$ and $Re=1000$. It can be seen that the non-smoothness of the 128×128 grid causes artificial non-smoothness in the streamlines near the kink in the grid lines for $Re=1000$. Inaccuracy of the discretization on the grid of Figure 9 is to be expected with the method chosen due to the presence of Christoffel symbols, which involve second derivatives of the co-ordinate mapping. More smooth grids are needed, like the grid in Figure 11, constructed with a biharmonic grid generator.[44,45] A generating system of higher order, like the biharmonic grid generator allows

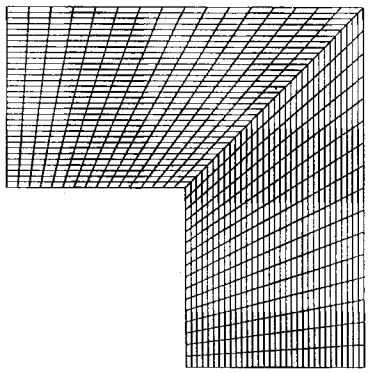

Figure 9. A non-smooth grid in an L-shaped channel

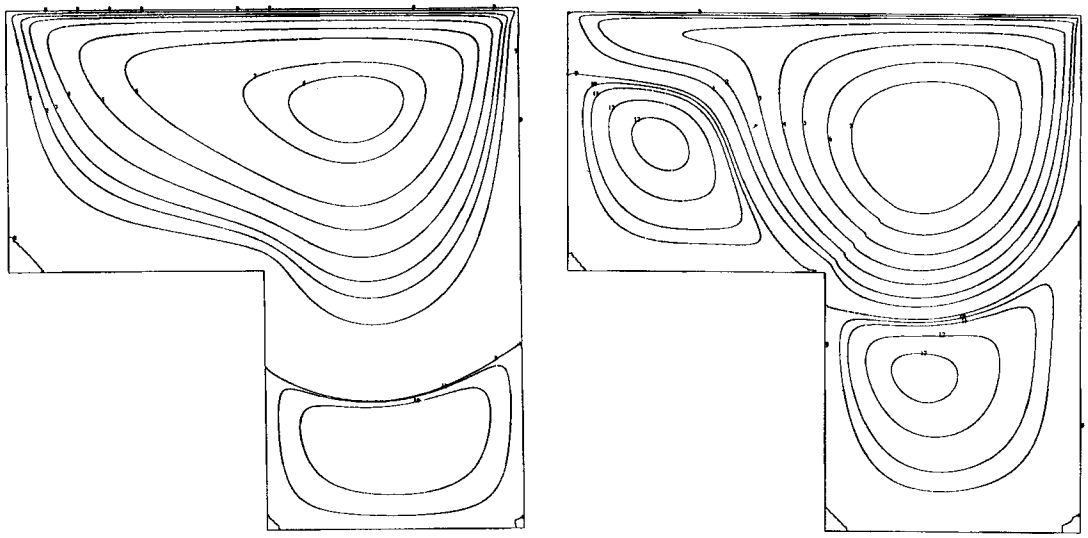

Figure 10. Streamlines for $Re = 100$ and $Re = 1000$ for an L-shaped cavity with the grid of Figure 9, 128×128 cells

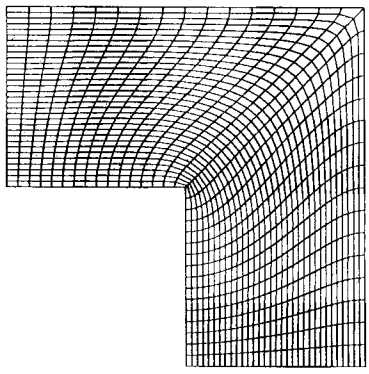

Figure 11. A smooth grid, in an L-shaped channel obtained with a biharmonic grid generator

more boundary conditions. Co-ordinate line angles are specified to be orthogonal at the boundary. (With a Laplace grid generator we also obtained smooth grids.) Figures 12 and 13 present streamlines and isobars for $Re=100$ and $Re=1000$, respectively. Local maximum and minimum values of the stream function Ψ_{max} and Ψ_{min} are presented for all grids together with their co-ordinates (x^1_{min}, x^2_{min}) and (x^1_{max}, x^2_{max}) in Table V. From Figure 13 it can be seen that the

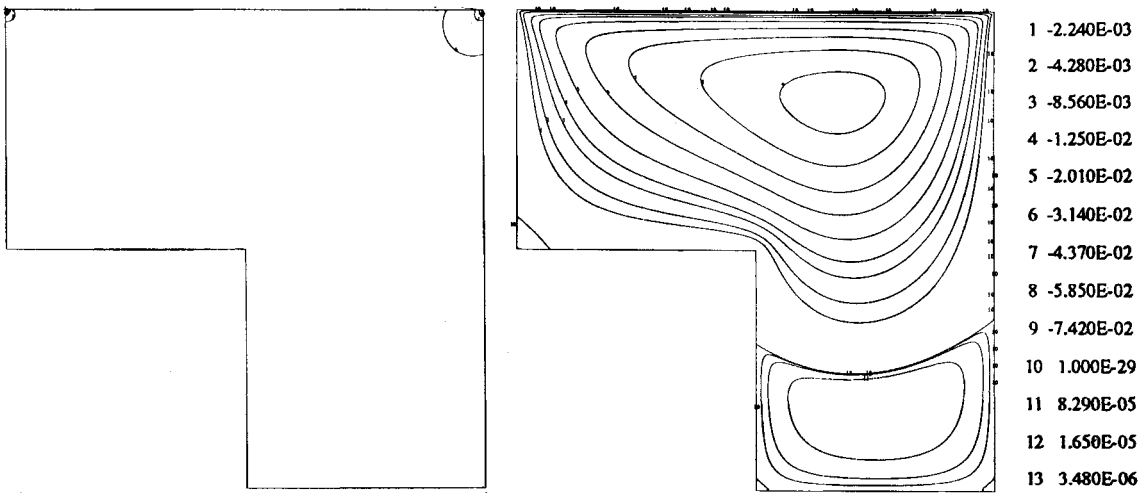

Figure 12. Isobars and streamlines an L-shaped cavity for $Re=100$ with the grid of Figure 11; 256×256 cells

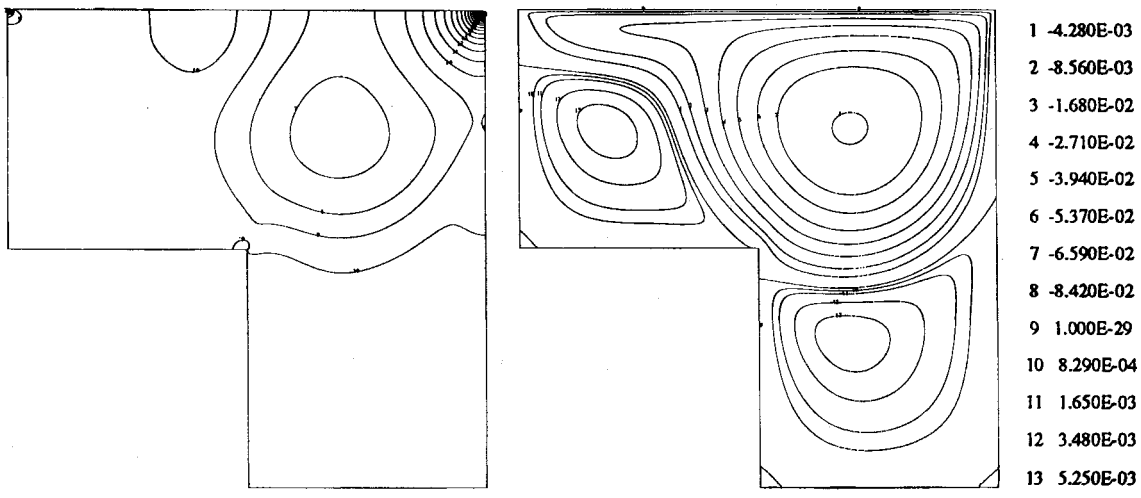

Figure 13. Isobars and streamlines for an L-shaped cavity for $Re=1000$ with the grid of Figure 11; 256×256 cells

Table V. Minimum and maximum stream function values in vortex centres and their position for all grids, L-shaped cavity, for both Reynolds numbers; grids similar to Figure 11 (for $Re = 100$ the finest grid consists of 256×256 cells.)

L-Shape	$Re = 100$		$Re = 1000$		
	Min	Max	Min	Max ($x^1 < 0{\cdot}5$)	Max ($x^1 > 0{\cdot}5$)
32×32					
Ψ	$-8{\cdot}1183 \times 10^{-2}$	$3{\cdot}3308 \times 10^{-4}$	$-6{\cdot}1571 \times 10^{-2}$	$4{\cdot}3821 \times 10^{-3}$	$3{\cdot}5184 \times 10^{-3}$
x	0·6737	0·7518	0·7326	0·1904	0·6589
y	0·8184	0·1720	0·7326	0·6895	0·2521
64×64					
Ψ	$-8{\cdot}1073 \times 10^{-2}$	$2{\cdot}7953 \times 10^{-4}$	$-7{\cdot}3215 \times 10^{-2}$	$5{\cdot}2854 \times 10^{-3}$	$6{\cdot}3619 \times 10^{-3}$
x	0·6679	0·7599	0·7026	0·1845	0·6604
y	0·8134	0·1747	0·7503	0·7289	0·2886
128×128					
Ψ	$-8{\cdot}0915 \times 10^{-2}$	$2{\cdot}6312 \times 10^{-4}$	$-8{\cdot}3419 \times 10^{-2}$	$6{\cdot}7005 \times 10^{-3}$	$5{\cdot}8084 \times 10^{-3}$
x	0·6763	0·7643	0·6983	0·1825	0·6855
y	0·8092	0·1747	0·7464	0·7525	0·3009
256×256					
Ψ	$-8{\cdot}0859 \times 10^{-2}$	$2{\cdot}5814 \times 10^{-4}$	$-8{\cdot}5392 \times 10^{-2}$	$6{\cdot}2021 \times 10^{-3}$	$6{\cdot}2503 \times 10^{-3}$
x	0·6734	0·7658	0·6947	0·1819	0·6877
y	0·8127	0·1713	0·7488	0·7505	0·3069
ε	0·0626	1·929	—	—	—
512×512					
Ψ	—	—	$-8{\cdot}5425 \times 10^{-2}$	$6{\cdot}4022 \times 10^{-3}$	$6{\cdot}2712 \times 10^{-3}$
x	—	—	0·6938	0·1822	0·6868
y	—	—	0·7509	0·7515	0·3089
ε	—	—	0·0386	3·126	0·333

flow at $Re = 1000$ has two stream function extrema, one for $x^1 < 0{\cdot}5$ and one for $x^1 > 0{\cdot}5$. Both are given in Table V. In order to judge accuracy as well as possible a 512×512 grid is needed for $Re = 1000$. One should keep in mind that the moving part of boundary Γ_2 is then discretized with 256 cells, like in the first two testcases. The results obtained on the 256×256 grid and the 512×512 grid are identical to a satisfactory extent. For $Re = 100$ the finest grid is a 256×256 grid. The error measure ε is defined for the finest grid as in (8).

Figure 14(a) shows the u^1 velocity profile along line CL_1 for $Re = 100$; Figure 14(b) gives the u^2 velocity profile along CL_2. Figure 15(a) shows u^1 along line CL_1 for $Re = 1000$, Figure 15(b) presents u^2 along CL_2. The velocity profiles predicted on the finest grid are given in tabulated form in Table VI for $Re = 100$ and in Table VII for $Re = 1000$, in which 14 reference points for reproduction of the profiles are given. At $(x^1, x^2) = (0{\cdot}5, 0{\cdot}5)$ a singular point occurs. For $Re = 1000$ it is inspected by giving, for all grids the pressure along the line $x^1 = 0{\cdot}5$ and the pressure along the line $x^2 = 0{\cdot}5$ in Figure 16. A large change in pressure, found to be similar on the three finest grids, can be observed at the singular point.

Finally, Table VIII presents μ_{nit} and ν_{nit} for the L-shape. Figure 17 presents the L_2-norm of the residual versus the number of iterations for the L-shaped cavity for $Re = 100$ and $Re = 1000$. As expected the slopes of all lines in this figure are almost identical. This indicates the level-independent convergence rates of the multigrid method used. The average reduction factors for $Re = 100$ are very good, only 15 iterations are needed to reduce the residual by 8 orders of

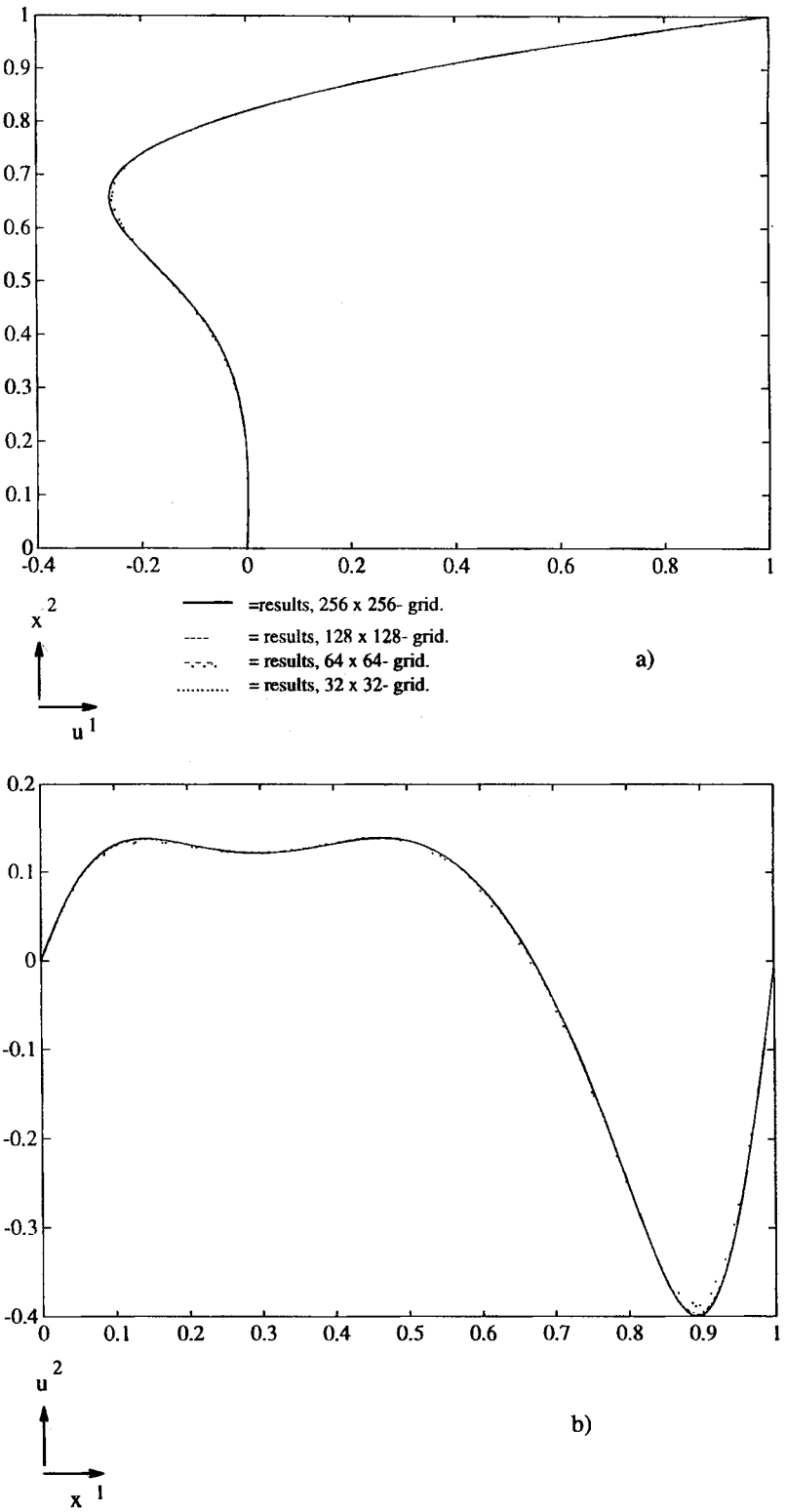

Figure 14. Velocity profiles for $Re = 100$ in the L-shaped cavity: (a) u^1 along CL_1; (b) u^2 along CL_2

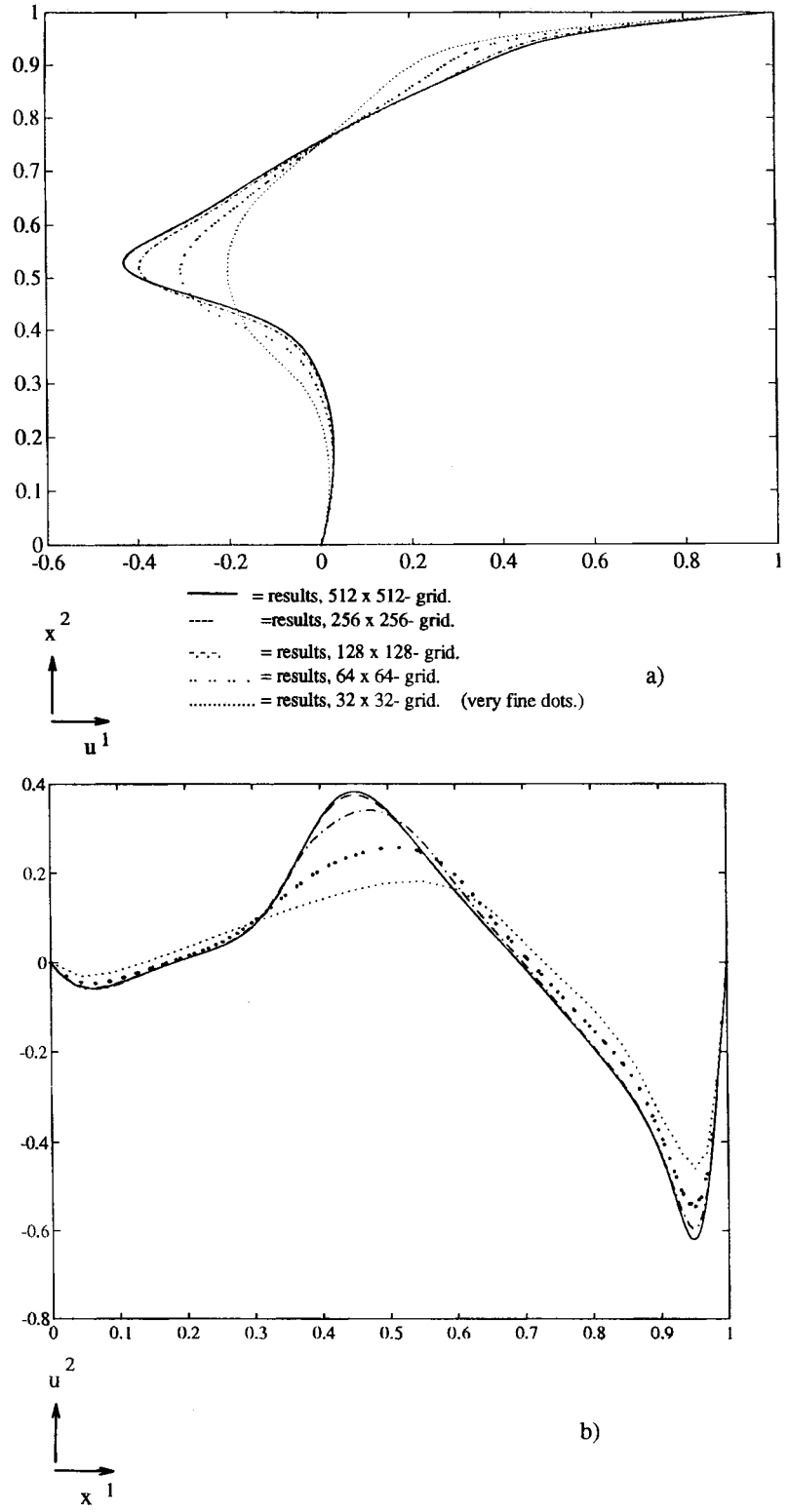

Figure 15. Velocity profiles for $Re = 1000$, L-shaped cavity: (a) u^1 along CL_1; (b) u^2 along CL_2

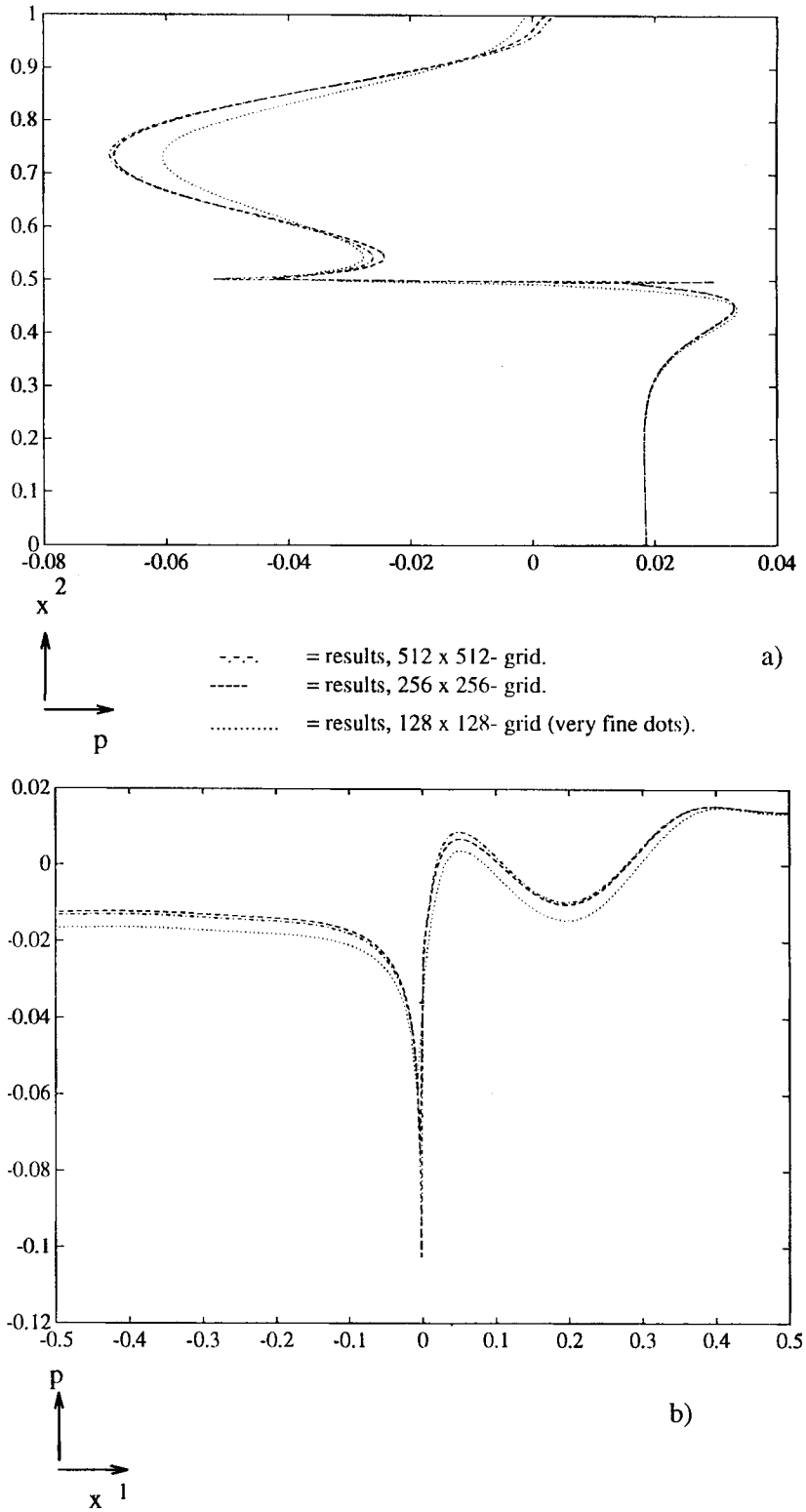

Figure 16. Pressure profiles along the line $x^1 = 0{\cdot}5$ (a), and line $x^2 = 0{\cdot}5$ (b), both through the singular point $(x^1, x^2) = (0{\cdot}5, 0{\cdot}5)$ for $Re = 1000$.

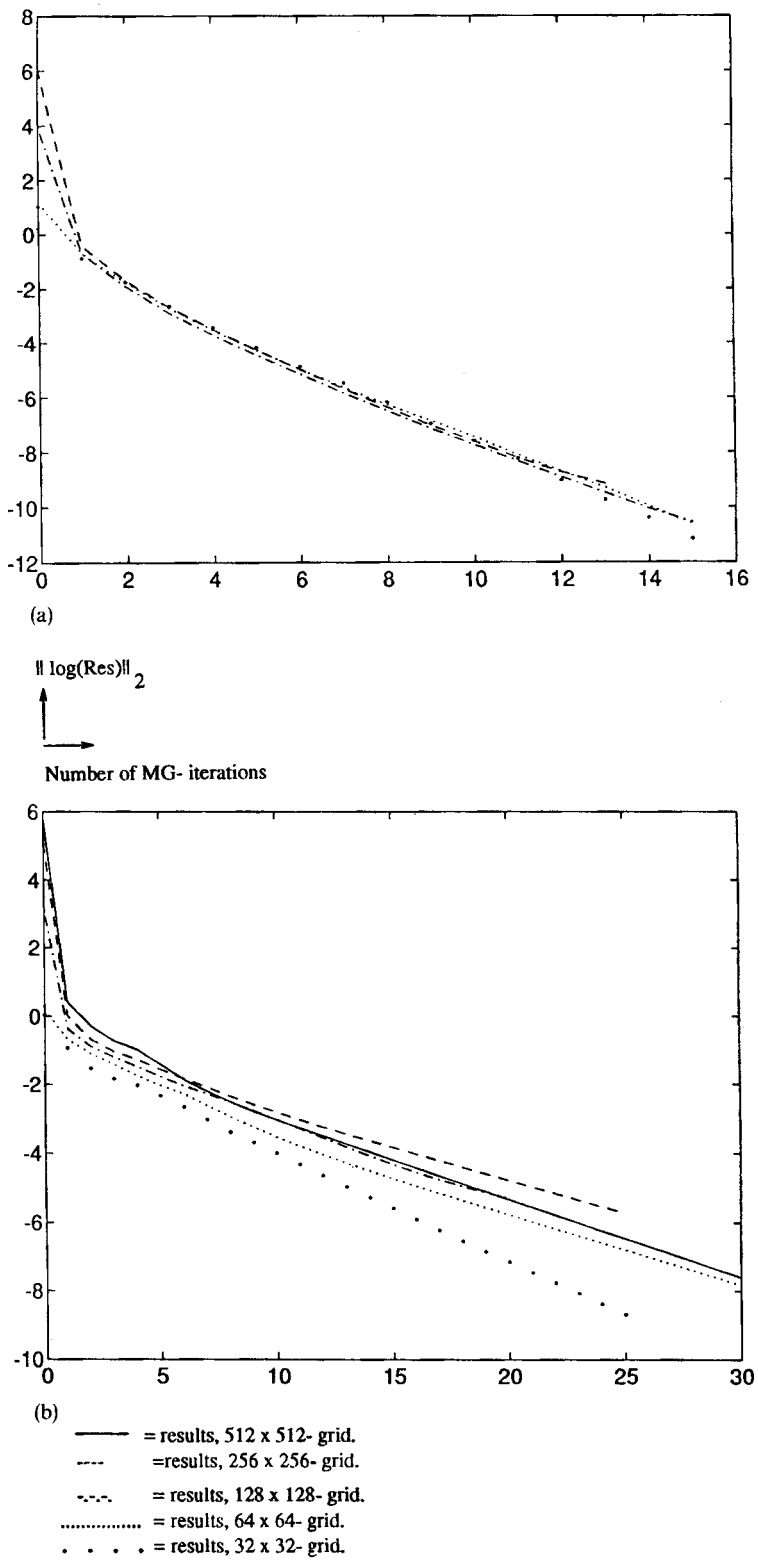

Figure 17. The L_2-norm of the residual versus the number of iterations for the F(1, 1)-cycle (1 pre-, 1 post-smoothing) for $Re = 100$ (a) and $Re = 1000$ (b) for the L-shaped cavity.

Table VI. Selected Cartesian components (u^1, u^2) along lines CL_1 and CL_2 for an L-shaped cavity, $Re = 100$

L-shape, $Re = 100$			
x^1	u^1	x^2	u^2
$1{\cdot}391067 \times 10^{-1}$	$1{\cdot}427423 \times 10^{-3}$	$4{\cdot}999769 \times 10^{-2}$	$9{\cdot}035508 \times 10^{-2}$
$3{\cdot}249394 \times 10^{-1}$	$-2{\cdot}673955 \times 10^{-2}$	$9{\cdot}866030 \times 10^{-2}$	$1{\cdot}299809 \times 10^{-1}$
$4{\cdot}496036 \times 10^{-1}$	$-9{\cdot}856450 \times 10^{-2}$	$1{\cdot}403140 \times 10^{-1}$	$1{\cdot}379881 \times 10^{-1}$
$5{\cdot}024952 \times 10^{-1}$	$-1{\cdot}467907 \times 10^{-1}$	$2{\cdot}924033 \times 10^{-1}$	$1{\cdot}215604 \times 10^{-1}$
$5{\cdot}689500 \times 10^{-1}$	$-2{\cdot}121597 \times 10^{-1}$	$4{\cdot}691068 \times 10^{-1}$	$1{\cdot}387131 \times 10^{-1}$
$6{\cdot}387627 \times 10^{-1}$	$-2{\cdot}584130 \times 10^{-1}$	$5{\cdot}298618 \times 10^{-1}$	$1{\cdot}280727 \times 10^{-1}$
$6{\cdot}509587 \times 10^{-1}$	$-2{\cdot}609123 \times 10^{-1}$	$6{\cdot}011217 \times 10^{-1}$	$8{\cdot}317737 \times 10^{-2}$
$6{\cdot}582105 \times 10^{-1}$	$-2{\cdot}613650 \times 10^{-1}$	$7{\cdot}020829 \times 10^{-1}$	$-4{\cdot}919975 \times 10^{-2}$
$6{\cdot}776128 \times 10^{-1}$	$-2{\cdot}580779 \times 10^{-1}$	$8{\cdot}846614 \times 10^{-1}$	$-3{\cdot}980422 \times 10^{-1}$
$7{\cdot}103055 \times 10^{-1}$	$-2{\cdot}364301 \times 10^{-1}$	$8{\cdot}926683 \times 10^{-1}$	$-3{\cdot}995829 \times 10^{-1}$
$8{\cdot}010405 \times 10^{-1}$	$-5{\cdot}735737 \times 10^{-2}$	$9{\cdot}004891 \times 10^{-1}$	$-3{\cdot}975273 \times 10^{-1}$
$8{\cdot}441612 \times 10^{-1}$	$8{\cdot}892393 \times 10^{-2}$	$9{\cdot}252045 \times 10^{-1}$	$-3{\cdot}641550 \times 10^{-1}$
$9{\cdot}043458 \times 10^{-1}$	$3{\cdot}615964 \times 10^{-1}$	$9{\cdot}501776 \times 10^{-1}$	$-2{\cdot}843395 \times 10^{-1}$
$9{\cdot}524048 \times 10^{-1}$	$6{\cdot}458474 \times 10^{-1}$	$9{\cdot}841114 \times 10^{-1}$	$-1{\cdot}055517 \times 10^{-1}$

Table VII. Selected Cartesian components (u^1, u^2) along lines CL_1 and CL_2 for an L-shaped cavity, $Re = 1000$

L-shape, $Re = 100$			
x^1	u^1	x^2	u^2
$1{\cdot}008904 \times 10^{-1}$	$2{\cdot}214952 \times 10^{-2}$	$1{\cdot}012788 \times 10^{-1}$	$-4{\cdot}598057 \times 10^{-2}$
$1{\cdot}012788 \times 10^{-1}$	$2{\cdot}220298 \times 10^{-2}$	$2{\cdot}001027 \times 10^{-1}$	$8{\cdot}319043 \times 10^{-3}$
$3{\cdot}083983 \times 10^{-1}$	$-3{\cdot}958527 \times 10^{-4}$	$3{\cdot}002279 \times 10^{-1}$	$8{\cdot}151612 \times 10^{-2}$
$3{\cdot}559005 \times 10^{-1}$	$-2{\cdot}947157 \times 10^{-2}$	$4{\cdot}024018 \times 10^{-1}$	$3{\cdot}277335 \times 10^{-1}$
$4{\cdot}004040 \times 10^{-1}$	$-8{\cdot}499573 \times 10^{-2}$	$4{\cdot}496036 \times 10^{-1}$	$3{\cdot}822040 \times 10^{-1}$
$4{\cdot}790068 \times 10^{-1}$	$-3{\cdot}279580 \times 10^{-1}$	$5{\cdot}024953 \times 10^{-1}$	$3{\cdot}360547 \times 10^{-1}$
$5{\cdot}224505 \times 10^{-1}$	$-4{\cdot}280438 \times 10^{-1}$	$5{\cdot}505747 \times 10^{-1}$	$2{\cdot}495101 \times 10^{-1}$
$5{\cdot}295923 \times 10^{-1}$	$-4{\cdot}297859 \times 10^{-1}$	$7{\cdot}001215 \times 10^{-1}$	$-1{\cdot}130681 \times 10^{-2}$
$6{\cdot}003576 \times 10^{-1}$	$-3{\cdot}051670 \times 10^{-1}$	$9{\cdot}380253 \times 10^{-1}$	$-6{\cdot}011807 \times 10^{-1}$
$6{\cdot}549982 \times 10^{-1}$	$-1{\cdot}944255 \times 10^{-1}$	$9{\cdot}481664 \times 10^{-1}$	$-6{\cdot}196227 \times 10^{-1}$
$7{\cdot}116315 \times 10^{-1}$	$-8{\cdot}681319 \times 10^{-2}$	$9{\cdot}547680 \times 10^{-1}$	$-6{\cdot}092847 \times 10^{-1}$
$8{\cdot}233341 \times 10^{-1}$	$1{\cdot}566785 \times 10^{-1}$	$9{\cdot}701669 \times 10^{-1}$	$-4{\cdot}919449 \times 10^{-1}$
$9{\cdot}185696 \times 10^{-1}$	$4{\cdot}041500 \times 10^{-1}$	$9{\cdot}851177 \times 10^{-1}$	$-2{\cdot}647262 \times 10^{-1}$
$9{\cdot}740718 \times 10^{-1}$	$7{\cdot}053604 \times 10^{-1}$	$9{\cdot}950405 \times 10^{-1}$	$-8{\cdot}754424 \times 10^{-2}$

Table VIII. Average and asymptotic reduction factors for an L-shaped cavity problem

Reynolds number	100		1000	
	μ_{nit}	ν_{nit}	μ_{nit}	ν_{nit}
32×32 grid	0·184	0·198	0·479	0·494
64×64 grid	0·195	0·252	0·566	0·623
128×128 grid	0·198	0·265	0·595	0·669
256×256 grid	0·204	0·252	0·588	0·644
512×512 grid	—	—	0·529	0·592

magnitude. Also for $Re = 1000$ the average reduction factors are satisfying. Due to the hybrid difference scheme they are not as good as the factors for lower Reynolds numbers, but they are level-independent. This means that almost the same number of iterations is needed to reduce a residual by several orders of magnitude for small and very large grids. The multigrid solver is also robust: all reduction factors are well below one. The smoother can deal with cells of varying size coming from a mesh generator. Furthermore, it is found that the code is insensitive to large variations of underrelaxation parameters for low Reynolds numbers, and that for the higher Reynolds number small variations are allowed.

4. CONCLUSIONS

The benchmark solutions show that our code is a reliable solver for the two-dimensional incompressible Navier–Stokes equations on sufficiently smooth non-orthogonal grids; the benchmark solutions proposed in Reference 6 are solved with satisfying accuracy. For low Reynolds numbers very accurate results are obtained with a small number of grid points. For higher Reynolds numbers the effect of a hybrid discretization scheme can be observed for a small number of unknowns in the high-velocity regions. When larger grids (128×128) are used this effect is reduced. The flow in an L-shaped cavity is proposed as another interesting benchmark problem, and good results are obtained for this problem; velocity profiles and streamfunction values converge fast to accurate solutions. The multigrid solution algorithm is robust and efficient. For problems in different geometries similar reduction factors were obtained. The code is insensitive to small variations of underrelaxation parameters.

REFERENCES

1. W. Rodi, S. Majumdar and B. Schönung, 'Finite volume methods for two-dimensional incompressible flows with complex boundaries', *Comput. Methods Appl. Mech. Eng.*, **75**, 369–392 (1989).
2. C. M. Rhie, W. L. Chow, 'A numerical study of the turbulent flow past an isolated airfoil with trailing-edge separation', *AIAA J.*, **21**, 1525–1532 (1983).
3. C. M. Rhie 'A pressure based Navier–Stokes solver using the multigrid method', *AIAA Paper 86-0207*, 1986.
4. M. Perić, 'A finite volume method for the prediction of three-dimensional fluid flow in complex ducts', *Ph. D. Thesis*, University of London, London, 1985.
5. I. Demirdzic and M. Peric, 'Finite volume method for prediction of fluid flow in arbitrarily shaped domains with moving boundaries', *Int. j. numer. methods fluids*, **10**, 771–790 (1990).
6. I. Demirdzic, Z. Lilek and M. Peric, 'Fluid flow and heat transfer test problems for non-orthogonal grids: bench-mark solutions', *Int. j. numer. methods fluids*, **15**, 329–354 (1992).
7. E. Dick and J. Linden, 'A multigrid flux-difference splitting method for steady incompressible Navier–Stokes equations'. in P. Wesseling (ed.), *Proc. 8th GAMM Conf. on Numerical Methods in Fluid Mechanism*, Notes on Numerical. Fluid Mechanics, vol. 29, Vieweg, Braunschweig, 1990 pp. 99–108.
8. E. Dick and J. Linden, 'A multigrid method for steady incompressible Navier–Stokes equations based on flux difference splitting', *Int. j. numer. methods fluids*, **14**, 1311–1323 (1992).
9. F-S. Lien and M. A. Leschziner, 'Multigrid convergence acceleration for complex flow including turbulence', in W. Hackbusch, U. Trottenberg (eds), *Multigrid Methods III*, Series of Numerical Mathematics, Vol. 98, Birkhäuser, Basel, 1991, pp. 277–288.
10. I. P. Jones, Experience with the vectorisation of some fluid flow prediction codes on the Harwell Cray I, in *Vectorisation on Computer Programs with Application to Computational Fluid Dynamics*, Lecture notes on Numerical Fluid Mechanics, vol. 8, Vieweg, Braunschweig, 1984, pp. 244–253.
11. D. Kwak, J. L. C. Chang, S. P. Shanks and S. R. Chakravarthy, 'A three dimensional incompressible Navier–Stokes flow solver using primitive variables', *AIAA J.*, **24**, 390–396 (1986).
12. S. E. Rogers and D. Kwak, 'Upwind differencing scheme for the time-accurate incompressible Navier–Stokes equations', *AIAA J.*, **28**, 253–262 (1990).
13. M. Rosenfeld, D. Kwak and M. Vinokur, 'A fractional step solution method for the unsteady incompressible Navier–Stokes equations in generalized coordinate systems', *J. Comput. Phys.*, **94**, 102–137 (1991).
14. M. Rosenfeld, D. Kwak, 'Multigrid acceleration of a fractional step solver in generalized coordinate systems', *AIAA Paper 92-0185*, 1992.
15. M. Rosenfeld and D. Kwak, 'Numerical solution of unsteady incompressible viscous flows in generalized moving coordinate systems', *AIAA Paper 89-0466*, 1989.

16. T. Ikohagi and B. R. Shin, 'Finite difference schemes for steady incompressible Navier–Stokes equations in general curvilinear coordinates', *Comput. Fluids*, **19,** 479–488 (1991).
17. T. Ikohagi, B. R. Shin and H. Daiguji, 'Application of an implicit time-marching scheme to a three-dimensional incompressible flow problem in curvilinear coordinate systems', *Comput. Fluids*, **21,** 163–175 (1992).
18. K. Katsuragi and O. Ukai, 'Navier–Stokes equations on a curvilinear co-ordinate system', in P. Wesseling (ed.), *Proc. of the 8th GAMM Conf. on Numerical Methods in Fluid Mechanics*, Notes on Numerical Fluid Mechanics, Vol. 29, Vieweg, Braunschweig, 1990, pp. 233–241.
19. S. Koshizuka, Y. Oka and S. Kondo, 'A staggered differencing technique on boundary-fitted curvilinear grids for incompressible flows along curvilinear or slant walls', *Comput. Mech.*, **7,** 123–136 (1990).
20. R. S. Bernard and H. Kapitza, 'How to discretize the pressure gradient for curvilinear MAC grids', *J. Comput. Phys.*, **99,** 288–298 (1992).
21. W. Shyy and T. C. Vu, 'On the adoption of velocity variable and grid system for fluid flow computation in curvilinear coordinates', *J. Comput. Phys.*, **92,** 82–105 (1991).
22. W. Shyy and C-S. Sun, 'Development of a pressure-correction/staggered-grid based multigrid solver for incompressible recirculating flows', *Comput. Fluids*, **22,** 51–76 (1992).
23. L. Davidson and P. Hedberg, 'Mathematical derivation of a finite volume formulation for laminar flow in complex geometries', *Int. j. numer. methods fluids*, **9,** 531–540 (1989).
24. H. Miyata and Y. Yamada, 'A finite difference method for 3D flows about bodies of complex geometry in rectangular co-ordinate systems', *Int. j. numer. methods fluids*, **14,** 1261–1287 (1992).
25. A. E. Mynett, P. Wesseling, A. Segal and C. G. M. Kassels, 'The ISNaS incompressible Navier–Stokes solver: invariant discretization', *Appl. Scientific Res.*, **48,** 175–191 (1991).
26. A. Segal, P. Wesseling, J. van Kan, C. W. Oosterlee and C. G. M. Kassels, 'Invariant discretization of the incompressible Navier–Stokes equations in boundary fitted co-ordinates', *Int. j. numer. methods fluids*, **15,** 411–426 (1992).
27. P. Wesseling, A. Segal, J. van Kan, C. W. Oosterlee and C. G. M. Kassels. 'Finite volume discretization of the incompressible Navier–Stokes equations in general coordinates on staggered grids', *Comput. Fluids Dyn. J.*, **1,** 27–33 (1992).
28. C. W. Oosterlee and P. Wesseling, 'A multigrid method for a discretization of the incompressible Navier–Stokes equations in general coordinates', in J. B. Vos, A. Rizzi and I. L. Ryhming (eds), *Proc. 9th GAMM Conf. on Numerical Methods in Fluid Mechanic*, Ser. Notes on Numerical Fluid Mechanics, vol. 35, Vieweg, Braunschweig, 1992, pp. 99–106.
29. C. W. Oosterlee and P. Wesseling, 'A multigrid method for an invariant formulation of the incompressible Navier–Stokes equations in general coordinates', *Comm. Appl. Numer. Methods*, **8,** 721–734 (1992).
30. S. V. Patankar and D. B. Spalding, 'A calculation procedure for heat and mass transfer in three-dimensional parabolic flows', *Int. J. Heat Mass Transfer*, **15,** 1787–1806 (1972).
31. S. V. Patankar, *Numerical Heat Transfer and Fluid Flow*, McGraw-Hill, New York, 1980.
32. M. C. Thompson and J. H. Ferziger, 'An adaptive multigrid technique for the incompressible Navier–Stokes equations', *J. Comput. Phys.*, **82,** 94–121 (1989).
33. R. Aris, *Vectors, Tensors and the Basic Equations of Fluid Mechanics*, Prentice-Hall, Englewood Cliffs, NJ, 1962.
34. I. S. Sokolnikoff, *Tensor Analysis*, Wiley, Englewood Cliffs, NJ, 1964.
35. C. W. Oosterlee and P. Wesseling, 'A robust multigrid method for a discretization of the incompressible Navier–Stokes equations in general coordinates, *Report 92-14*, Faculty of Technical Mathematics and Informatics, Delft University of Technology, Delft, 1992; *Impact of Comp. Sci. and Eng.* (to appear).
36. A. Brandt, 'Guide to multigrid development', in W. Hackbusch and U. Trottenberg (eds), *Multigrid Methods*, Lecture Notes in Mathematics, Vol. 960, Springer, Berlin, 1982, pp. 220–312.
37. W. Hackbusch, *Multi-grid Methods and Applications*, Springer, Berlin, 1985.
38. P. Wesseling, *An Introduction to Multigrid Methods*, Wiley, Chichester, 1992.
39. S. P. Vanka, 'Block-implicit calculation of steady turbulent recirculating flows', *Int. J. Heat Mass Transfer*, **28,** 2093–2103 (1985).
40. D. S. Joshi and S. P. Vanka, 'Multigrid calculation procedure for internal flows in complex geometries', *Numer. Heat Transfer*, **20,** 61–80 (1991).
41. U. Ghia, K. N. Ghia and C. T. Shin, 'High-*Re* solutions for incompressible flow using the Navier–Stokes equations and a multigrid method', *J. Comput. Phys.*, **48,** 387–411 (1982).
42. S. P. Vanka, 'Block-impact multigrid solution of Navier–Stokes equations in primitive variables. *J. Comput. Phys.*, **65,** 138–158 (1986).
43. C. Y. Perng and R. L. Street, 'A coupled multigrid-domain-splitting technique for simulating incompressible flows in geometrically complex domains', *Int. j. numer. methods fluids*, **13,** 269–286 (1991).
44. J. F. Thompson, Z. U. A. Warsi and C. W. Mastin, *Numerical Grid Generation*, North-Holland, Amsterdam, 1985.
45. K. Stüben and J. Linden, 'Multigrid methods: an overview with emphasis on grid generation processes', in J. Haüser (ed.), *Proc. 1st Int. Conf. on Numerical Grid generation*, Pineridge Press, Swansea, 1986.
46. I. Demirdzic, A. D. Gosman, R. Issa and M. Peric, 'A calculation procedure for turbulent flow in complex geometries', *Comput. Fluids*, **3,** 251–273 (1987).
47. D. Rayner, 'Multigrid flow solutions in complex two-dimensional geometries', *Int. j. numer. methods fluids*, **13,** 507–518 (1991).